Effect of actively targeted copolymer coating on solid tumors eradication by gold nanorods-induced hyperthermia

Roberto Puleio[a], Mariano Licciardi[b]*, Paola Varvarà[b], Cinzia Scialabba[b], Giovanni Cassata[a], Luca Cicero[b], Gennara Cavallaro[b], Gaetano Giammona[b]

[a]Istituto Zooprofilattico Sperimentale della Sicilia "A. Mirri", Via Gino Marinuzzi 3, 90100 Palermo, Italy.

[b]Department of Scienze e Tecnologie Biologiche Chimiche e Farmaceutiche (STEBICEF), Università degli Studi di Palermo, 90123 Palermo, Italy.

*Corresponding author: mariano.licciardi@unipa.it; Department of Scienze e Tecnologie Biologiche Chimiche e Farmaceutiche (STEBICEF), Università degli Studi di Palermo, 90123 Palermo, Italy.

Abstract

Efforts in the field of anticancer therapy are increasingly focusing on the development of localized and selective treatments. Photothermal therapy (PTT) can lead to a spatially confined death of cancer cells, exploiting an increasing in temperature generated after UV-NIR irradiation of peculiar materials. Herein, a new actively targeted gold-based drug delivery system, named PHEA-LA-Fol-AuNRs/Iri, was explored for hyperthermia and chemotherapy colon cancer treatment. Gold nanorods were stabilized using a folate-derivative of poly(N-2-hydroxyethyl)-D,L-aspartamide (PHEA-LA-PEG-FA) as coating agent and then loaded with the antineoplastic drug irinotecan (Iri). The efficacy of empty and irinotecan-bearing systems was investigated *in vitro* on human colon cancer (HCT116) cell line, as well as *in vivo*, employing a xenograft mouse model of colon cancer. After laser treatment, both nanostructures tested induced a considerable deceleration in tumor growth overtime, achieving the total eradication of the cancer when PHEA-LA-Fol-AuNRs/Iri was intratumorally administered. Biodistribution data showed that the polymer coated nanorods were able to preferentially accumulate in the tumor site. Considering the excellent stability in aqueous media, the capacity to reach the tumor site and, finally, the *in vivo* efficacy, PHEA-LA-Fol-AuNRs/Iri might be recommended as an effective tool in the chemotherapy and PTT of colon cancer.

Keywords

gold nanorods; hyperthermia; photothermal therapy; solid tumor; magnetic resonance imaging, folic acid

1. Introduction

Photothermal therapy (PTT) is progressively emerging as one of the most promising tools in selective cancer treatment, with a special focus on metastasis management (Zou et al., 2016). The key principle of PTT consists in the controlled and spatially localized increasing in temperature, which is responsible for cellular damage by means of proteins denaturation and enhanced permeability of biomembranes, eventually leading to cancer cell death (Camerin et al., 2005; Jori and Spikes, 1990; Lepock, 2003). In particular, depending on the temperature reached in a given district, heat production in PTT can be distinguished in hyperthermia (42-46°C), which causes mild to moderate cytotoxic effects, and thermal ablation (>50°C), consisting in a drastic cell damage via coagulative necrosis and membrane fracture (O'Neal et al., 2004; Yang et al., 2015). The innate susceptibility of cancer cells against small risings in temperature, along with the possibility to exploit nanomaterials-driven PTT, configure this approach as particularly suitable for tumor-selective therapies (Hildebrandt et al., 2002).

To fulfill this intention, several nanomaterials have already been proposed, such as gold colloids (nanorods, nanoshells, nanocages) (Melancon et al., 2011; Qiu et al., 2017; Yu et al., 2016; Zhang et al., 2016), copper-based nanocrystals (Wang et al., 2015), carbon nanotubes (Liang et al., 2014), graphene-based nanomaterials (Fiorica et al., 2017; Jiang et al., 2014; Mauro et al., 2017; Nicolò Mauro et al., 2016) porphyrin-based nanoassemblies (Lovell et al., 2011). All of these nanomaterials have the capability to generate heat in the surrounding area, due to the relaxation of the excitation energy absorbed during light exposure (Chen and Cai, 2015; Sortino, 2012). In virtue of their nanometric size, preferential tumor accumulation can be achieved through passive targeting, also known as Enhanced Permeability and Retention (EPR) effect (Maeda and Matsumura, 1989; Matsumura and Maeda, 1986). In addition, the decoration with site specific ligands, endows these

nanomaterials active targeting abilities, magnifying the amount of nanoconstructs in the target site and decreasing their abundance in the undesired areas (Craparo et al., 2014; Sinha et al., 2006).

Among the aforementioned materials, gold colloids gained increasing attention in the field of nanomedicine and, especially, in the cancer treatment and diagnosis branch (Chen et al., 2018; Zhang et al., 2015). With this aim, in the last few decades, colloidal gold has been extensively employed because of its peculiar features, such as biological inertia and the possibility to tailor size and shape during the synthesis procedure. The most appealing characteristics of nanosized gold are however attributable to its Surface Plasmon Resonance (SPR) phenomenon, responsible for its relevant optical properties. Above all, gold nanorods appear to be an excellent option in PTT, due to their ability to exert hyperthermia effect when excited by NIR light (650−900 nm wavelength). In fact, it has been shown that NIR radiation has a better penetration power in comparison to shorter wavelength radiations, allowing to reach even subdermal layers of the skin, thus exploiting hyperthermia effect on a deeper level (Li Volsi et al., 2017; Lowery et al., 2006; Weissleder, 2001).

Keeping in mind this scenario, in the present work, gold nanorods coated with an amphiphilic copolymer, bearing active targeting ligands and loaded with the antineoplastic drug irinotecan were produced, characterized and tested *in vivo* as hyperthermia agents in solid tumor eradication. The polymeric derivative employed, named PHEA-LA-PEG-FA, was obtained by grafting to the α,β-poly(N-2-hydroxyethyl)-D,L-aspartamide (PHEA) backbone, lipoic acid (LA) molecules and polyethylene glycol (PEG) chains carrying folate (FA) in their termini. PHEA is a biocompatible poliaminoacidic synthetic polymer deriving from polysoccinimide (PSI), widely used for a large variety of applications in drug delivery (Castelli et al., 2000; Craparo et al., 2015; Licciardi et al., 2013b; N. Mauro et al., 2016), whilst, lipoic acid residues linked to the polyaminoacidic main chain were used as hydrophobic moieties, as well as pendant disulfide functions, crucial elements for gold surface coating (Gobin et al., 2010; Pensa et al., 2012). Further decoration with folate molecules was aimed to endow the nanosystems active targeting capabilities towards tumors that express high levels

of folate receptor (FR), such as colon, lung, breast, ovary carcinomas and others (Parker et al., 2005; Reddy and Low, 1998). On the other hand, 2KD PEG chains were supposed to act as spacer for FA, potentially increasing its availability for the ligand-receptor interaction. Moreover, pegylation is responsible for the constitution of a hydrophilic shell, which provides gold nanorods stability in physiological fluids and longer circulation times in the bloodstream (Li and Huang, 2010). The copolymer coated nanorods were then loaded with the topoisomerase I inhibitor irinotecan, an antineoplastic drug widely adopted in colorectal cancer therapy (Fuchs et al., 2006; Fujita et al., 2015). After physicochemical characterization and *in vitro* studies, the efficacy of empty and drug loaded systems, either with or without laser treatment, was finally evaluated *in vivo* on colorectal cancer xenograft models.

2. Materials and Methods

2.1. Materials

α,β-poly(N-2-hydroxyethyl)-D,L-aspartamide (PHEA) and amino-polyethylene glycol folate-amide (PEG-FA) were synthesized as already reported (Licciardi et al., 2013a; Mendichi et al., 2003). (±)-α-lipoic acid (LA), N,N′-dicyclohexylcarbodiimide (DCC), 4-(dimethylamino)pyridine (DMAP), bis(4-nitrophenyl) carbonate (BNPC), hexadecyltrimethylammonium bromide (CTAB ≥96%), silver nitrate, L-ascorbic acid, sodium borohydride, Gold(III) chloride hydrate, acetone, methanol, ethanol, diethylether and anhydrous N,N-dimethylformamide were purchased from Sigma-Aldrich. Sephadex G-25 gel permeation resin was purchased from Fluka (Switzerland). SpectraPor dialysis tubing were purchased from Spectrum Laboratories, Inc. (UK). Milli-Q water (resistivity 18.2 MΩ·cm at 25°C) was used for the whole set of experiments.

Human colon cancer cells HCT116 were cultured in Dulbecco's Modified Eagle Medium (DMEM) supplemented with 10% v/v of fetal bovine serum (FBS), L-glutamine (2mM), streptomycin (100mg mL^{-1}), penicillin G (100units mL^{-1}), amphotericin B (2.5μg mL^{-1}), all purchased from Euroclone, and incubated al 37°C in humidified environment with 5% of CO_2.

Eukitt® acrylic mounting medium was purchased from O. Kindler GmbH. Ki-67 rabbit monoclonal (CRM325) and Caspase-3 cleaved rabbit polyclonal primary antibodies (CP229) were purchased from Biocare Medical and used after 1:100 dilution. LSAB Kit and 3-3'-diaminobenzidine tetrahydrochloride were purchased from Dako Corp. (Santa Barbara, CA). All the reagents employed were analytical grade if not otherwise specified.

2.2. Synthesis of CTAB-AuNRs

The preparation of AuNRs was carried out following a silver-assisted seed-mediated growth procedure in CTAB (Li Volsi et al., 2017). Gold seeds were synthesized dispersing 25μL of 0.05M $HAuCl_4$ solution in CTAB 0.1M (4.7mL), followed by rapid reduction by means of 300μL $NaBH_4$ 0.01M, under vigorous stirring. In a typical synthesis pathway, 500μL of 0.05M $HAuCl_4$ solution and 950μL of HCl 1M are added in 50 mL CTAB 0.1M and left to equilibrate for few minutes. The subsequent addition of 600μL $AgNO_3$ 0.01M, 400μL of ascorbic acid 0.1M and 120μL of freshly prepared seeds, finally leads to the CTAB-AuNRs formation.

2.3. Synthesis of PHEA-LA-PEG-FA copolymer

PHEA-LA-PEG-FA copolymer synthesis was performed by modifying a previously reported two-step protocol (Li Volsi et al., 2018). During the first step, PHEA-LA was synthesized dissolving lipoic acid (LA) in DMF (39.14mg, 0.19mmol in 1.5mL) and allowing it to react with a solution of DCC (47.46mg, 0.23mmol) and DMAP (28.1mg, 0.23mmol) in 1mL of the same solvent. After 1h at 25°C under stirring, the reaction mixture was added dropwise to a solution of PHEA in DMF (200mg, 1.265mmol of repeating units in 2.5mL) and maintained for 18h at 30°C, under stirring. The reaction flask content was then filtered, and the solvent removed under vacuum at 30°C by using rotary evaporator. Precipitation and washings of the obtained derivative were accomplished in acetone/diethyl ether mixture 1:1 v/v and the copolymer PHEA-LA was retrieved as a dried powder (yield: 223mg). The second step has led to the synthesis of PHEA-LA-PEG-FA. In particular, BNPC

(38.33mg, 0.126mmol) dissolved in 1mL DMF was added dropwise into a PHEA-LA solution (200mg in 2.5mL DMF) and kept for 2.5h at 40°C under stirring. Subsequently, PEG-FA (Licciardi et al., 2013a) (302.4mg, 0.126mmol in 1.5mL DMF) was slowly added to the reaction mixture and left to react for 18h at 25°C under stirring. The product was precipitated in acetone, washed in acetone/methanol mixture 1:1 v/v and dried under vacuum. The collected powder was dissolved in 2mL of water and the purification was completed through gel permeation chromatography using Sephadex G25 as separating gel. After freeze drying, PHEA-LA-PEG-FA was recovered as a yellowish lyophilizate with a 152.5% yield based on the starting PHEA-LA amount. ^{1}H NMR (300MHz, D_2O, 25°C, δ): 2.82 (m, 2H PHEA, -CH-C$\underline{H_2}$-CONH-), 3.36 (t, 2H PHEA, -NH-C$\underline{H_2}$-CH_2-OH), 3.66 (t, 2H PHEA,-CH_2-C$\underline{H_2}$-OH), 4.72 (m, 1H PHEA, -NH-C$\underline{H}$-CO-CH_2-), δ 1.39 (m, 2H LA, -HO-CO-CH_2-CH_2-CH_2-C**H₂**-cCH_2-CH_2-CH_2-S-S-), 1.59 (4H LA, -HO-CO-C**H₂**-C**H₂**-CH_2-CH_2-cCH-CH_2-CH_2-S-S-), 1.97 (m, 2H LA, -HO-CO-CH_2-CH_2-CH_2- CH_2-cCH-C**H₂**-CH_2-S-S-), 2.23 (m, 2H LA-HO-CO-C**H₂**-CH_2-CH_2-CH_2-cCH-CH_2-CH_2-S-S-), 2.54 (m, 2H LA-HO-CO-CH_2-CH_2-CH_2-CH_2-cCH-CH_2-C**H₂**-S-S-), 3.70 (m,176H PEG2000,-NH-CH_2-CH_2-(O-C**H₂**-C**H₂**)44-), δ 6.69-7.52 4H FA, phenyl group.

2.4. Preparation of PHEA-LA-Fol and PHEA-LA-Fol/Iri AuNRs

Preparation of PHEA-LA-Fol-AuNRs required the removal of the cationic surfactant excess from CTAB-AuNRs (20mg of Au) by washing them twice with double-distilled water and retrieving the product after centrifugation (8500rpm, 20min, 23°C). AuNRs coating was then achieved by adding dropwise a dispersion of PHEA-LA-PEG-FA in ultrapure water (200mg in 20mL) to the nude AuNRs and incubating the mixture for 18h at 37°C in Orbital Shaker. The drug loaded systems PHEA-LA-Fol-AuNRs/Iri were produced following an analogous protocol, aside from the addition of irinotecan into the coating dispersion. More specifically, a solution of irinotecan hydrochloride in double-distilled water (40mg, 0.642mmol in 20mL) was treated with triethylamine (6.42mmol) in order to produce irinotecan free base (Iri). The drug was then slowly dropped into a dispersion of PHEA-LA-

PEG-FA (200mg in 20mL) in the same solvent and kept for 1h at 25°C. This mixture was subsequently added to the washed AuNRs, incubated (18h, 37°C) and purified from irinotecan excess through SpectraPor dialysis tubing (12-14KD MWCO) obtaining PHEA-LA-Fol-AuNRs/Iri after freeze-drying.

2.5. Dynamic Light Scattering analysis, Zeta potential measurement and gold content determination

PHEA-LA-Fol-AuNRs and PHEA-LA-Fol-AuNRs/Iri were characterized in terms of hydrodynamic diameter (Z-Average), PDI and Zeta potential, using a Malvern Zetasizer NanoZS instrument, fitted with a 532 nm laser at a fixed scattering angle of 173°. Each sample was dispersed in ultrapure water at the concentration of 0.25 mg mL^{-1} and analyzed at 25°C. The intensity-average hydrodynamic diameter and polydispersity index (PDI) were obtained by cumulant analysis of the correlation function. The Zeta potential (mV) was calculated from the electrophoretic mobility using the Smoluchowsky relationship and assuming that Ka ≫1 (where K and a are the Debye-Hückel parameter and particle radius, respectively). The gold content of empty and drug loaded systems was determined through Spectroquant® Gold Test (Merck, Germany) and expressed as percentage w/w.

2.6. Scanning electron microscopy (SEM)

The morphology and size of PHEA-LA-Fol-AuNRs-IT were visualized using a scanning electron microscope, ESEM Philips XL30. A drop of a PHEA-LA-Fol-AuNRs/Iri water dispersion (10μL, 0.001mg·mL^{-1}) was laid onto a TEM copper grid and dried overnight.

SEM imaging was performed after deposition of the grid on a double-sided adhesive tape, previously applied on a stainless-steel stub.

2.7. Estimation of drug payload into PHEA-LA-Fol-AuNRs/Iri and stability study

PHEA-LA-Fol-AuNRs/Iri irinotecan cargo was investigated via Agilent Infinity 1290 HPLC apparatus equipped with a Gemini® 5 µm C6-Phenyl column (Phenomenex), following an already described method (Fiorica et al., 2017), with some variations. Analyses were performed at 25°C by using a ternary mixture of PBS pH 2.7/acetonitrile/methanol 60:20:20 v/v/v as mobile phase with a flow rate of 1mL/min and the diode array detector fixed at 254nm. Samples were prepared extracting the free drug from a well-known amount of PHEA-LA-Fol-AuNRs/Iri, employing mobile phase as solvent and keeping the samples incubating for 3h under vigorous stirring. The dispersions obtained were filtered through 0.22µm RC filters before being injected (25µL injection volume). Drug loading was calculated as the w/w percentage of irinotecan on the total weight of the system, by comparison with a standard curve of irinotecan free base (linearity range= 10^{-4}- 0.5 mg mL^{-1}; R^2 = 0.99998).

PHEA-LA-Fol-AuNRs/Iri stability studies were performed by UV-VIS measurements using a Shimadzu UV-2400 spectrophotometer. 5mg of freeze-dried product were dispersed in 10 mL of ultrapure water and UV-vis spectra were acquired weekly after 1:5 v/v dilution checking the overall stability for 1 month.

2.8. PHEA-LA-Fol-AuNRs/Iri drug release studies

Drug release studies were carried out using phosphate buffer solution pH 7.4 or acetate buffer solution pH 5.5 as release media. PHEA-LA-Fol-AuNRs/Iri (7.8mg) or an equivalent amount of irinotecan free base (1mg) were put in dialysis tubes (SpectraPor 2KD MWCO), immersed in buffer solution (20mL) and maintained at 37°C under continuous orbital shaking at 100rpm (Benchtop 808C Incubator Orbital Shaker model 420) for 24h. At established intervals, 1mL of external medium was withdrawn and replaced with the same volume of fresh buffer solution. The irinotecan content into the aliquots collected was calculated through HPLC analysis and the release profiles were determined plotting the drug released (percentage w/w on the total drug payload) versus incubation times.

2.9. Hyperthermia studies

PHEA-LA-Fol-AuNRs and PHEA-LA-Fol-AuNRs/Iri dispersions with different gold concentrations (10, 20, 40 μg/mL Au) were placed in a 24 well-plate and treated with an 810nm diode laser (GBox 15A/B by GIGA Laser) with the power set at 3.5×10^{-3} W/mm^3 or 7×10^{-3} W/mm^3. Temperatures were recorded at fixed intervals ranging from 0 to 300 seconds by using a fiber optic temperature probe (±1°C sensitivity) and reported as a function of the exposure time.

2.10. Cytotoxicity assay

The cytotoxicity studies were carried out by the tetrazolium salt (MTS) assay, using a commercially available kit (Cell Titer 96 Aqueous One Solution Cell Proliferation assay, Promega). Human colon cancer (HCT116) cell line was used for the experiments. Cells were seeded at a density of $2.5 \cdot 10^4$ cells/well in 96-well plates with supplemented medium (DMEM) and allowed to adhere for 24h. Therefore, cells were incubated for 24 and 48h with PHEA-LA-Fol-AuNRs, PHEA-LA-Fol-AuNRs/Iri and free irinotecan (solubilized in DMSO), used as positive control, at a drug concentration per well equal to 3, 6, 12, 24, 36 μg mL^{-1}. Untreated cells were used as negative control. After 24 and 48 h of incubation, DMEM was replaced with 100μL of fresh medium and 20μL of MTS solution was added to each well. Plates were incubated for an additional 2h at 37°C. Then, the absorbance at 492nm was measured using a microplate reader (PlateReader AF2200, Eppendorf). The viability was expressed as percentage obtained from the ratio between each sample with respect to their negative control (100% of cell viability).

2.11. Tumor xenografts

All animal experiments were performed following the protocols "Guide for the Care and Use of Laboratory Animals" published by the National Institutes of Health. Male athymic nude mice (Fox1nu/nu) were purchased from Envigo, Udine, Italy. Mice were acclimated for 1 week before starting this study. Animals were kept in a light- and temperature-controlled environment and

provided with food and water ad libitum. All experiments described within this section, were performed in the Istituto Zooprofilattico Sperimentale della Sicilia "A.Mirri" (Italy).

To generate a tumor xenograft, $5 \cdot 10^6$ human colon cancer (HCT116) cells in 200μL of PBS were subcutaneously injected to the lower back of 4-week old male mice. Mice were randomly divided into treatment or control groups in each experiment after that the tumors were appeared and palpable.

2.12. In vivo antitumor activity

When tumors became palpable (around $180mm^3$), mice were randomly divided into ten groups, each group containing five mice. More specifically, animals in groups 1 and 2 received intratumoral injection of saline solution (0.05 mL, 0.9%). Animals in groups 3 and 4 received intratumoral injection of empty PHEA-LA-Fol-AuNRs (0.05 mL, 25mg mL^{-1} of nanoparticles, dispersed in saline solution, corresponding to 4mg Kg-^{1} of Au). Animals in group 5 received intraperitoneal injection of empty PHEA-LA-Fol-AuNRs (0.05mL, 25mg mL^{-1} of empty nanoparticles, dispersed in saline solution, corresponding to 4mg Kg^{-1} of Au). Animals in groups 6 and 7 received intratumoral injection of irinotecan (0.05mL, 6.5mg mL^{-1} of drug, dispersed in saline solution, corresponding to 12.8mg Kg^{-1} of irinotecan). Animals in groups 8 and 9 received intratumoral injection of irinotecan loaded PHEA-LA-Fol-AuNRs (0.05mL, 50mg mL^{-1} of drug loaded nanoparticles, dispersed in saline solution, corresponding to 4 mg Kg^{-1} of Au and 12.8mg Kg^{-1} of irinotecan). Animals in groups 10 received intraperitoneal injection of irinotecan loaded PHEA-LA-Fol-AuNRs (0.05mL, 50mg mL^{-1} of drug loaded nanoparticles, dispersed in saline solution, corresponding to 4mg Kg^{-1} of Au and 12.8mg Kg^{-1} of irinotecan). Animals belonging to groups 2, 4, 5, 7, 9 and 10 were treated three times (every 3 days, until the end of experiment) for 20 seconds with a 810nm cold laser beam, set with a power of 7 Watt, with the aim to evaluate the capability of gold nanorods to eradicate tumor mass by means of hyperthermic effect.

Every 3 days, mice were weighted, the tumors were measured by external caliper and the tumor volume was calculated by the formula $V = L \cdot W^2 / 2$. Where, L is the longest diameter (in mm) of the tumor and W (in mm) is the longest perpendicular diameter with respect to L.

After 9 days mice were sacrificed and each tumor was excised, fixed and embedded in paraffin wax to perform histopathology and immunohistochemistry studies. This study was authorized by the Italian Ministry of Health (N.351-2017).

2.13. Magnetic Resonance Imaging

Magnetic Rresonance Imaging (MRI) was performed employing a 7 T horizontal bore PharmaScan 70/16 US scanner (Bruker, Ettlingen, Germany) equipped with a 23 mm transmit/receive volumetric coil. Prior to analysis, mice were anaesthetized using 2% isoflurane and then protected from hypothermia with the use of a hot water blanket. Mice respiration was monitored during the experiment. Before intratumoral injection of irinotecan and PHEA-LA-Fol-AuNRs/Iri, baseline scans were performed. A TE = 35.0 ms and a triggered T2_Turbo RARE sequence was selected for T2 imaging.

2.14. Biodistribution of nanosystems

To determine the biodistribution of the nanoparticles, free irinotecan and PHEA-LA-Fol-AuNRs/Iri were intraperitoneal administered to mice. The mice were grouped in six mice per group. Group 1 was treated with 6.5mg mL^{-1} of irinotecan dispersed in sterile saline solution. Group 2 was treated with 50mg mL^{-1} of PHEA-LA-Fol-AuNRs/Iri, corresponding to 6.5mg mL^{-1} of irinotecan, dispersed in sterile saline solution. After 24 and 48 h, three mice of each groups were sacrificed by cervical dislocation and heart, kidneys, liver, lungs, spleen and tumor were collected.

Organs and tumors withdrawn by mice were weighed and stored at -20°C and allowed to thaw at room temperature before processing. Each sample was used to extract irinotecan. For irinotecan extraction, tumors and organs were first washed twice with phosphate buffer to remove blood and

then suspended in 5mL of phosphate buffer at pH 2.6 and homogenized to extract the drug for 5 minutes. The homogenates were centrifuged, and supernatants were analyzed by HPLC for irinotecan quantification. Tumors of untreated mice were used as control.

2.15. Histology - Hematoxylin & Eosin staining

Routine histology (hematoxylin-eosin staining, H&E) was performed in order to evaluate basic histomorphological features of the specimens. 4 µm thick sections were obtained by formalin-fixed paraffin-embedded tissue that were set on slides treated with silane ((3-aminopropyl) triethoxysilane) in order to avoid detachment during staining. The preparations obtained were dried overnight in an oven at 37°C. It was proceeded with dewaxing by xylene for 20 min. After a descending alcohol series (100°, 95°, 75° and 50°), slides were washed in distilled water and then stained with hematoxylin and eosin. This was followed by the ascending scale of alcohols (50°, 75°, 95° and 100°) and clarification in xylene. After this phase the slides were mounted in Eukitt® acrylic mounting medium.

2.16. Immunohistochemistry

Ki67 and Caspase 3 cleaved investigation was assessed by immunohistochemistry. Sections (4 µm thick) were cut and stored at room temperature before use. After dewaxing, the slides were heated in a solution of sodium citrate (pH 6.0) at 96 °C for 20 min for antigen retrieval. Endogenous peroxidase activity was blocked with 3% w/v hydrogen peroxide in methanol for 30 min. Slides were treated with Background Sniper for 15 min and incubated for 1 h at RT with rabbit monoclonal Ki-67 and rabbit polyclonal anti Caspase-3 cleaved antibody. After incubation, the slides were rinsed three times with PBS for 5 minutes, and a secondary biotinylated immunoglobulin (LSAB) was applied for 30 minutes at room temperature. After two x 5-minute rinses with PBS, tissue sections were incubated in PBS for 1 hour at room temperature with streptavidin-horseradish peroxidase conjugate. All tissue sections were rinsed three times with TRIS-buffer saline (TBS), incubated with the chromogen 3-3'-

diaminobenzidine tetrahydrochloride (DAB) diluted 0.035% in TBS for 1 minute, rinsed in tap water, and counterstained with Mayer's hematoxylin. The specific primary antibodies were replaced with PBS or normal goat serum in tissue sections used as negative controls. The DAB-reaction developed a brown precipitate, when positive.

All immunostained sections were analyzed at a 200× magnification using Leica DMR microscope equipped with a Nikon DS-Fi1 digital camera.

Percentages of Caspase-3 cleaved and Ki-67 positive cells were quantified by using ImageJ software (ImageJ-NIH). This software calculates the percentage of positively-stained area (DAB-stained area) divided by total nuclear area, using a color deconvolution algorithm for separating the staining components (DAB and hematoxylin) and adaptive thresholding for nuclear area segmentation.

Statistical analysis was performed using Student's two-tailed t test. The criterion for statistical significance was $p < 0.05$.

3. Results and Discussion

3.1. Synthesis of PHEA-LA-PEG-FA

To ensure their stability in aqueous environment, gold-based nanostructures require to be coated with an appropriate hydrophilic coating (Turkevich et al., 1951). As reported elsewhere (Cavallaro et al., 2013), the use of hydrophilic polymers is particularly suitable for this purpose, being also responsible for the increasing in cytocompatibility and biocompatibility of gold colloids, thus allowing their employment *in vivo*. Another major requirement to obtain a successful coating of gold nanosystems, is the presence of functional groups able to establish stable bonds with the metal surface, such as thiols and amines (Gao et al., 2012; Grönbeck et al., 2000; Kumar et al., 2003). For these reasons, the copolymer used in this study was designed in order to satisfy all these prerequisites. Specifically, PHEA-LA-PEG-FA (Figure 1) convergent synthesis was articulated in three steps with isolation of the intermediates.

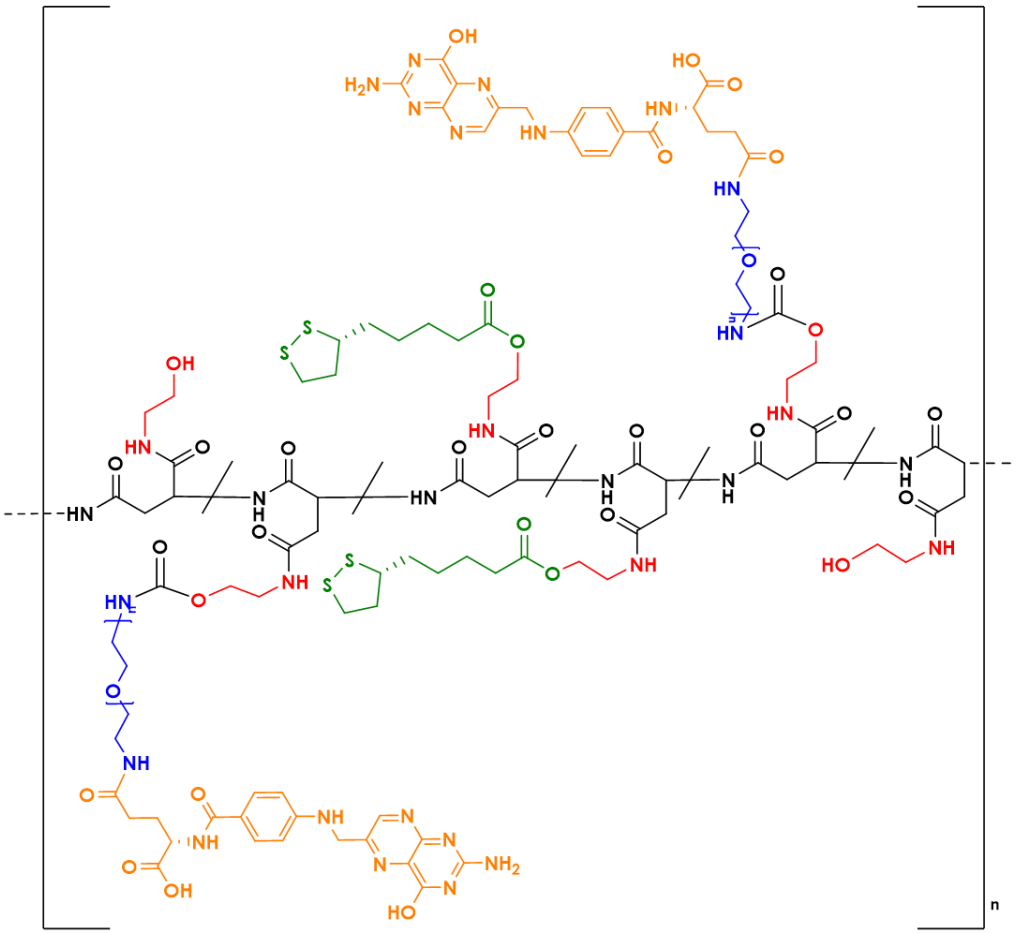

Figure 1. Structure of the derivative PHEA-LA-PEG-FA.

Concretely, the first step consisted in the grafting of lipoic acid chains on the polymeric backbone of α, β-poly (N-2-hydroxyethyl) -D, L-aspartamide (PHEA), through activation of the carboxyl groups of lipoic acid (LA) and subsequent esterification with the hydroxyl end groups of the PHEA backbone. Lipoic acid was here inserted with the aim of introducing disulfide groups, that provide a strong interaction with the gold surface. During the second step, the pegylation of folic acid molecules was accomplished through the formation of amide bonds between the carboxylic functions of folic acid (FA) previously activated and bis-amino-PEG chains (Licciardi et al., 2013a). This step was carried out using a molar ratio between folic acid molecules and PEG chains equal to 0.75, in order to reduce the possibility that two folic acid molecules could bind to the same PEG chain. The third and final step involved the synthesis of the copolymer PHEA-LA-PEG-FA (Figure 1) by grafting the PEG-FA chains onto the free hydroxyl end groups of PHEA-LA, previously activated by bis (4-

nitrophenyl) carbonate, generating a urethane bond. The grafting of PEG, enhanced the hydrophilicity of the PHEA backbone, improving the polymer stabilizing properties, whereas the folate pendant moieties were inserted to achieve an active targeting to the tumor site.

The copolymer thus obtained was characterized by ^{1}H NMR analysis to investigate the degrees of derivatization achieved. The derivatization degree percentage (DD%) in LA was calculated integrating the peaks attributed to the signals of 10H of LA (δ between 0.9 and 2.6) and it resulted equal to 6.36mol/mol%. The intense peak at δ 3.7 is typically produced by the 2H of each of the repetitive units of PEG and was therefore used for the determination of PEG degree of derivatization, corresponding to 5mol/mol%. Finally, a 4mol/mol DD% was estimated for FA, by taking into account the integrals of peaks at δ 7 and δ 7.2 (2H FA).

3.2. Preparation and characterization of coated AuNRs

CTAB-assisted gold nanorods synthesis leads to the formation of very stable gold cylindrical nanoparticles with a narrow size distribution. Nevertheless, the presence of the cationic surfactant as stabilizer does not allow their use in biomedical applications, due to CTAB prominent toxicity. The polymer coating it is able to replace CTAB on AuNRs surface thus preventing toxic effects and simultaneously acting as a protection towards aggregation. For this reason, the obtained derivative PHEA-LA-PEG-FA was used as coating agent, exploiting the well-known disulfide-gold chemistry. Lipoic acid moieties grafted on the polymer backbone are, in fact, responsible for the strong interaction between the coating polymer and gold nanorods, stabilizing the nanosystems in aqueous dispersions.

VIS-NIR spectroscopy of irinotecan-loaded AuNRs revealed no significant differences compared to drug-free systems (data not shown). Both systems appeared to be stable in aqueous media, without any sign of clusters formation. The stability of PHEA-LA-Fol-AuNRs/Iri after drug entrapment was evaluated through UV-VIS spectroscopic analysis. As shown in Figure 2, the absorption spectrum of

PHEA-LA-Fol-AuNRs/Iri dispersed in Milli-Q water, does not show signs of aggregation, as there is no significant red shift or widening of the SPR absorption band, in comparison with CTAB-AuNRs. Furthermore, it is possible to appreciate the presence of irinotecan loaded, by observing the peak at 350 nm.

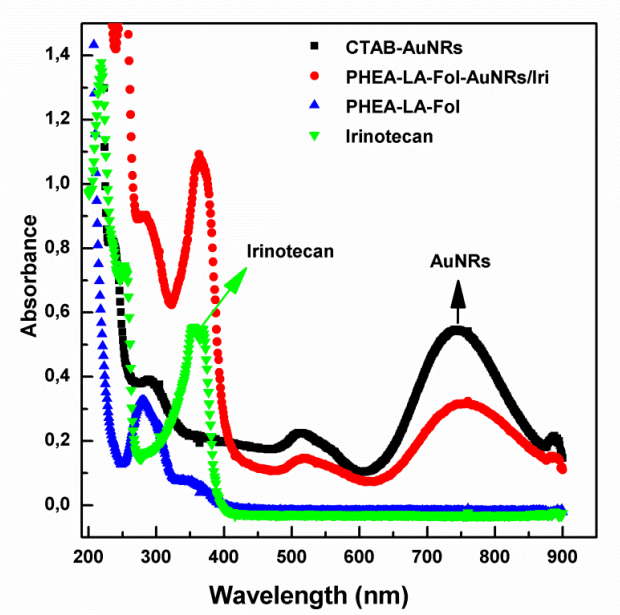

Figure 2. UV-VIS spectra of irinotecan free base (green inverted triangles), CTAB-AuNRs (black squares), PHEA-LA-PEG-FA (blue triangles), PHEA-LA-Fol-AuNRs/Iri (red circles).

Drug loading % was evaluated by HPLC analysis and it was found to be 12.86% (w/w). The polymer coated systems appeared able to load a considerable amount of drug, suggesting that PHEA-LA PEG-FA possesses the proper hydrophobic to hydrophilic balance to establish interactions with the drug (free base), as well as with the aqueous environment, thus stabilizing AuNRs. Hydrodynamic diameter and Zeta potential measurements (Table 1) showed that both empty and loaded systems are nanometric, moreover, the high and negative Zeta potential registered, proves that the cationic surfactant was successfully removed on nanorods surface, thus ensuring high stability towards aggregation and avoiding CTAB relate toxic effects. There were no significant variations between empty and loaded systems, either in terms of hydrodynamic diameter or Zeta potential, suggesting

370 that irinotecan is presumably loaded in the inner part of the coating, in proximity of the gold core, whilst the polymer chains acts as hydrophilic protective colloids, firmly anchored to the gold surface.

Table 1. Hydrodynamic diameters, polydispersity, Zeta potentials, irinotecan and gold content (percentage w/w) of CTAB-AuNRs, PHEA-LA-Fol-AuNRs and PHEA-LA-Fol-AuNRs/Iri.

Sample	Z-Average (nm)	PdI	Z potential	DL % (p/p)	Au % (p/p)
CTAB-AuNRs	78.6	0.511	14.6 ± 3.21	-	-
PHEA-LA-Fol-AuNRs	101.6	0.469	-13.9 ± 4.76	-	8.2
PHEA-LA-Fol-AuNRs/Iri	99.38	0.5	-21.6 ± 5.52	12.86	4.0

375 PHEA-LA-Fol-AuNRs and PHEA-LA-Fol-AuNRs/Iri were also characterized in terms of gold content, expressed as a percentage w/w. As depicted in Table 1, empty and loaded AuNRs possess a gold content high enough to allow very efficient hyperthermic effects, nevertheless, data reported a lower percentage w/w of gold in the irinotecan loaded system, probably attributable to the higher total weight of the loaded system, after drug incorporation.

380 The SEM morphological analysis carried out on drug loaded nanorods confirmed their rod shape as well as their nanometric size. Figure 3 illustrates that the actual size of PHEA-LA-Fol-AuNRs/Iri, is smaller than the hydrodynamic diameter registered. These data are consistent with the presence of a polymer shell surrounding the gold particles, thus magnifying the hydrodinamic diameter measured by DLS.

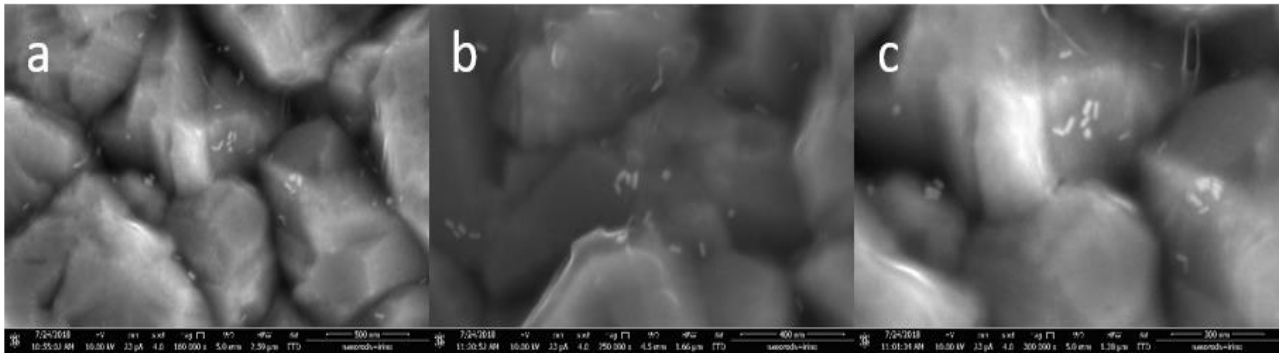

Figure 3. SEM microscopy on PHEA-LA-Fol-AuNRs/Iri using magnifications 160000X (a – Scale bar 500nm), 250000X (b – Scale bar 400nm), 300000X (c – Scale bar 300nm).

The evaluation of stability over time of irinotecan-bearing systems dispersed in ultrapure water (Figure 4), displayed no signs of aggregation, even after storage for one month at room temperature. In particular, the absence of red shift and the negligible variations of the width of the SPR band in the NIR region, demonstrated a good chemical-physical stability at least up to one month.

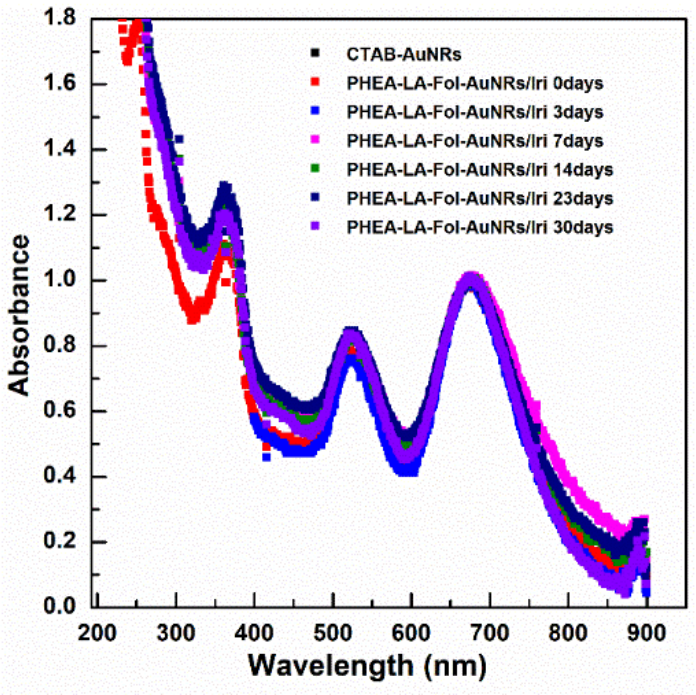

Figure 4. Stability study of PHEA-LA-Fol-AuNRs/Iri through UV-VIS analysis over time. Spectra acquired up to 1 month.

3.3. PHEA-LA-Fol-AuNRs/Iri drug release and hyperthermia studies

The ability of PHEA-LA-Fol-AuNRs/Iri to release the drug loaded was evaluated by using two different release media, simulating different compartments of the tumor environment. The release studies were carried out in PBS pH 7.4 which simulates extracellular and cytoplasmic fluids and in pH 5.5 acetate buffer mimicking the intratumoral and lysosome slightly acidic pH. The quantity of irinotecan released in each release medium was quantified at established time intervals.

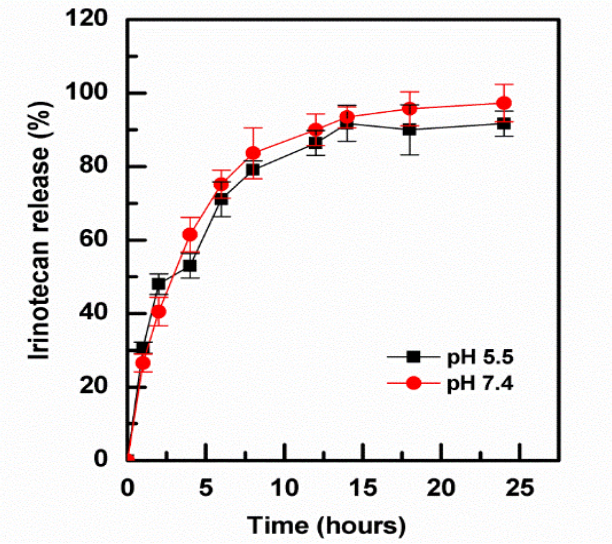

Figure 5. PHEA-LA-Fol-AuNRs/Iri release profiles. Irinotecan release from PHEA-LA-Fol-AuNRs/Iri in PBS pH 7.4 (red circles) and acetate buffer pH 5.5 (black squares).

Figure 5 shows the cumulative release% of irinotecan referred to the total amount of drug loaded in the systems, as a function of the incubation time. It is interesting to note that the system did not show a clear difference in the release of drug in the two media, settling after 12h between 80% and 90% of drug released in both release media used.

By exploiting the notorious ability of AuNRs to convert a NIR laser light into heat, hyperthermic properties of the prepared nanoconstructs were evaluated. Hence, the capability of the coated systems to induce a local thermic rise was studied after irradiation with an 810 nm diode laser beam, with a wavelength close to the SPR band of the AuNRs. Three different system concentrations were tested to investigate the dependence between the amount of gold and the increasing in temperature reached.

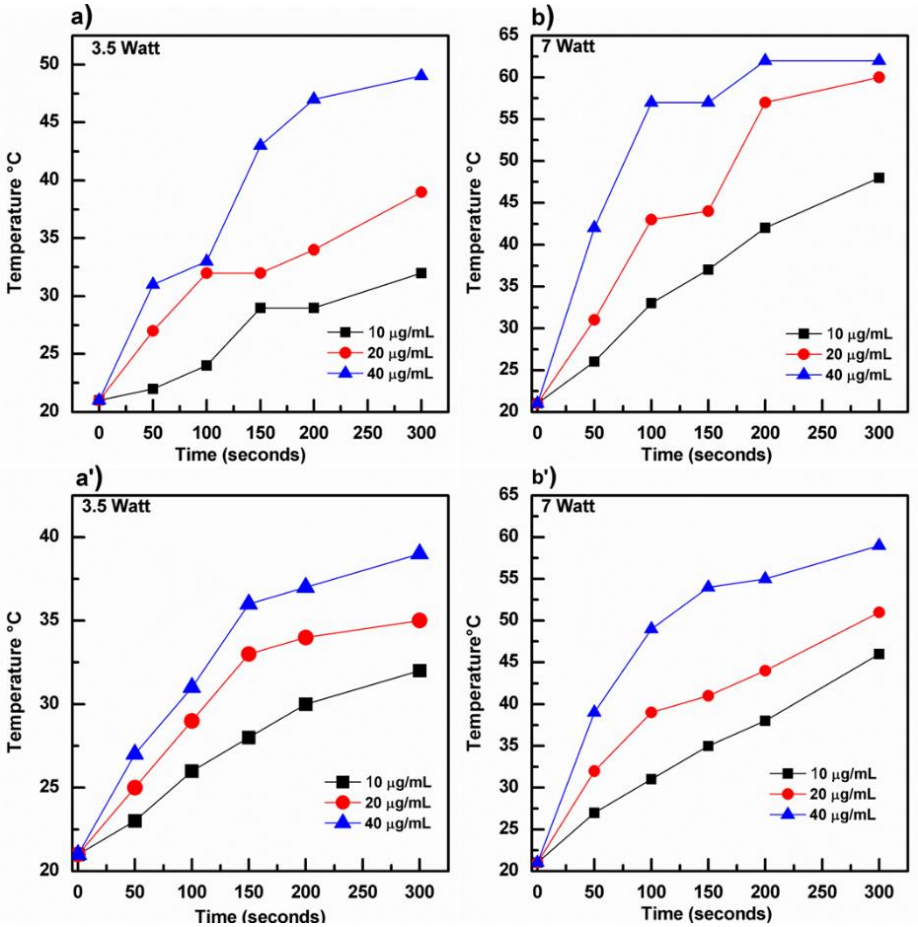

Figure 6. Hyperthermia evaluation. Temperatures recorded as a function of irradiation time of PHEA-LA-Fol-AuNRs (a-b) and PHEA-LA-Fol-AuNRs/Iri (a'-b'), employing three Au concentrations (10μg/mL-black squares; 20μg/mL-red circles; 40μg/mL-blue triangles) and using two different laser powers:3.5 W (a-a') and 7 W (b-b').

As reported in Figure 6, it is possible to observe that all the tested systems are able to cause a substantial increase in the temperature of the surrounding environment, which reaches values up to 63°C, therefore generating a hyperthermic effect which is function of the irradiation time. Considering the collected data, it is plausible to state that the increase in temperature shows different entities depending on different factors. First, the recorded temperature values appear to increase as the irradiation power increases. A similar trend is observed also accordingly to the rising in the concentration of the systems and therefore of the amount of gold employed. This latter phenomenon is due to the additive nature of the contributions of each particle that leads to a magnification of the

SPR. Furthermore, irinotecan containing systems showed a lower thermic rise in comparison with empty systems, presumably due to a shield effect exerted by the drug against the irradiation penetration or the excitation of the systems.

3.4. In vitro biological evaluations

In order to investigate the cytotoxicity of the nanosystems prepared, MTS colorimetric assay was carried out on human colon cancer (HCT116) cell line. The viability of the cultured cells was evaluated after 24 or 48h incubation with PHEA-LA-Fol-AuNRs, PHEA-LA-Fol-AuNRs/Iri and irinotecan free base, testing drug concentrations ranging from 3 to 36 μg mL^{-1}. As shown in Figure 7, the drug-free systems preserved their cytocompatibility after 24h incubation, with viability percentages ≥75% for all the concentrations tested, whereas, a mild cytotoxic effect after 48h incubation was showed, exclusively when highest concentrations were employed. Overall, the drug loaded nanorods induced a slightly stronger reduction in cell viability in comparison to irinotecan free base, with values flattening out after 48h incubation at the highest concentration (Figure 7b).

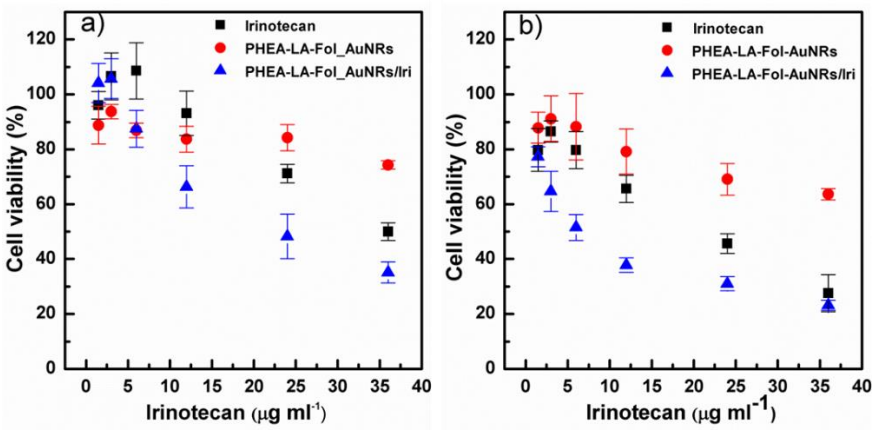

Figure 7. Cytotoxicity studies. Cell viability of HCT116 cell line incubated with irinotecan free base (black squares), PHEA-LA-Fol-AuNRs (red circles), PHEA-LA-Fol-AuNRs/Iri (blue triangles) after 24h (a), 48h (b).

This trend was confirmed by the values of IC50 after 24 and 48h and maximum inhibition percentages, reported in Table 2. It might be the case that the superior cytotoxicity displayed by the

PHEA-LA-Fol-AuNRs/Iri was due to the presence of the polymer coating, that could be able to promote the drug permeation into the cell, enhancing irinotecan efficacy.

Table 2. Irinotecan and PHEA-LA-Fol-AuNRs/Iri IC50 and I% after 24h and 48h tested on HCT116 cell line.

Sample	$IC50^{24h}$ (μg mL^{-1})	I%	$IC50^{48h}$ (μg mL^{-1})	I%
Irinotecan	35	50±1.9	21	72.5±2.1
PHEA-LA-Fol-AuNRs/Iri	21	65±3.2	7.1	76.8±1.6

3.5. In vivo antitumor activity and biodistribution

Current chemotherapy in cancer management is constantly manifesting the need of selective treatments in order to minimize drug related side effects. The use of actively targeted nanotechnologies, along with the employment of innovative local therapies, is supposed to overcome these drawbacks and therefore improve patients' outcomes. Thus, the *in vivo* efficacy of empty and loaded nanorods was tested, with or without laser irradiation, on xenograft-bearing athymic nude mice groups, as summarized in table 3.

Table 3. Mice groups subdivision for *in vivo* study.

Groups	Samples	Route of administration	Laser treatment	Dose (mg mL^{-1})
1	Saline solution	Intratumoral	-	-
2	Saline solution	Intratumoral	X	-
3	PHEA-LA-Fol-AuNRs	Intratumoral	-	25*
4	PHEA-LA-Fol-AuNRs	Intratumoral	X	25*
5	PHEA-LA-Fol-AuNRs	Intraperitoneal	X	25*
6	Irinotecan	Intratumoral	-	6.5
7	Irinotecan	Intratumoral	X	6.5

8	PHEA-LA-Fol-AuNRs/Iri	Intratumoral	-	50[*♯]
9	PHEA-LA-Fol-AuNRs/Iri	Intratumoral	X	50[*♯]
10	PHEA-LA-Fol-AuNRs/Iri	Intraperitoneal	X	50[*♯]

[*]Equal to 4 mg Kg^{-1} of gold nanorods. [♯]Equal to 12.8 mg Kg^{-1} of Irinotecan.

460 The response to the treatment was monitored registering mice body weights and tumor volumes throughout the entire duration of the experiments.

It is interesting to note that all the groups studied did not show any significant change in body weights (Figure 8b-b'), indicating the absence of severe acute toxicity during the whole experiment. Figure 8a illustrates an increase in tumor volumes measured in all control groups, including mice treated 465 with drug-free nanorods, but without laser irradiation. On the contrary, a statistically significant decreasing in tumor growth was observed in both groups receiving laser treatment, achieving the complete tumor eradication at day 6, after intratumoral injection of PHEA-LA-Fol-AuNRs. The present findings demonstrate that the coated systems can exert a considerably relevant therapeutic effect, even without chemotherapeutic drug.

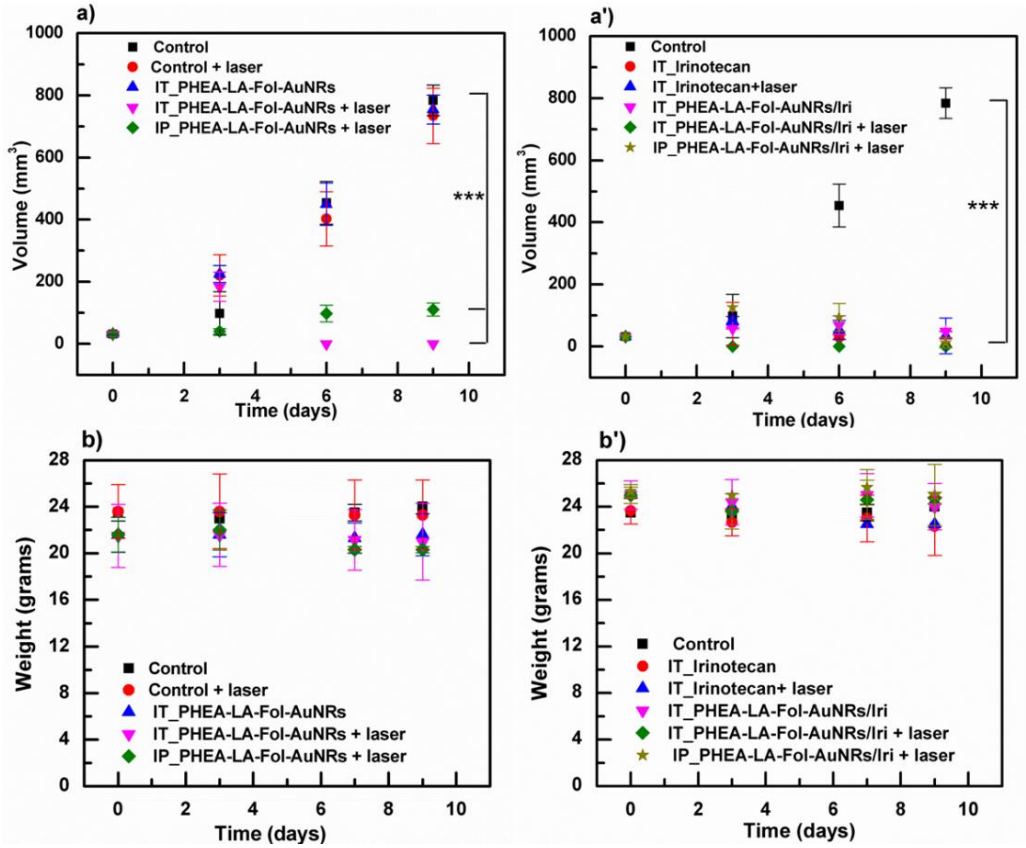

Figure 8. *In vivo* efficacy in tumor volume reduction and body weight records. Tumor volumes (a-a') and body weights (b-b') of mice after treatment with drug-free nanorods (a-b) and irinotecan-loaded nanorods (a'-b').

These results, not only underline PHEA-LA-Fol-AuNRs extraordinary hypertermic properties, but also suggest their potential use in colon cancer treatment without drug related side effects. Furthermore, a substantial deceleration in tumor progression was registered after laser treatment of mice that received intratumoral injection, as well as intraperitoneal administration. The hyperthermic efficacy of the irinotecan-free nanorods after parenteral administration, indicates the ability of nanostructures to reach the tumor target site. This evidence is likely be attributable to a contribution of two major factors. First, their nanometric size allow passive targeting. Secondly the folate moieties introduced in the coating polymer might provide active targeting towards the cancer site. All the irinotecan-loaded systems tested were capable of contrasting the tumor xenograft growth, as shown in Figure 8a', achieving once again the complete eradication of the cancerous mass at day 3, after

intratumoral injection of PHEA-LA-Fol-AuNRs/Iri. However, no significant differences in tumor volumes were recorded between the group treated exclusively with irinotecan and those that received PHEA-LA-Fol-AuNRs/Iri administration. Moreover, loaded nanorods seem to perform in a similar manner regardless the laser treatment, showing outcomes comparable to those obtained with the free drug. Both these evidences might suggest that irinotecan dosage chosen for these studies was already sufficient to promote a massive slowdown in tumor expansion, hence it was not possible to verify the potential synergistic effect of chemotherapy and hyperthermia.

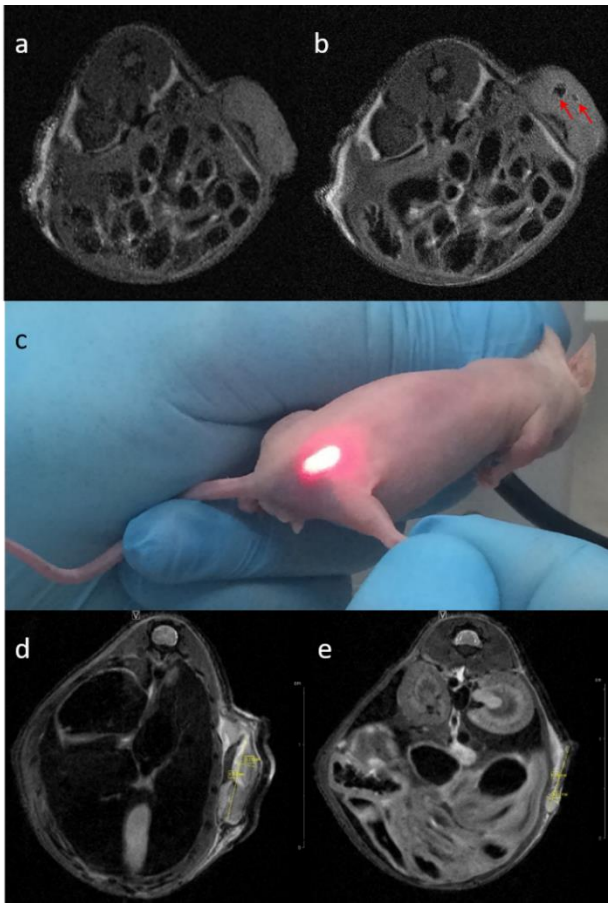

Figure 9. Monitoring of laser treatment efficacy via MRI. T2-weighted scans of a tumor-bearing mouse before intratumoral injection (a), after PHEA-LA-Fol-AuNRs/Iri intratumoral administration (b), 1 day post irradiation (d), 4 days post irradiation (e). Panel c shows the laser treatment procedure after injection.

To further confirm the efficacy of the laser-assisted thermoablation, tumors volume reduction was qualitatively followed through MRI imaging. Figure 9 shows the cross-section T2-weighted scans of a mouse, showing the tumor xenograft and its decreasing in volume over time. On completion of the PHEA-LA-Fol-AuNRs/Iri intratumoral injection (red arrows in panel b), mice were treated for 20 seconds with a 7Watt laser beam, carefully irradiating the tumor affected area, as illustrated in panel c. MRI scans were then acquired 1 and 4 days post-laser treatment (respectively Figure 9d and 9e). A significant progressive reduction in tumor size is clearly visible since the first day after laser irradiation, with xenograft volumes markedly decreasing at the end of the experiment.

Finally, nanoparticles and free irinotecan biodistribution studies were assessed to investigate their fate 24h and 48h after intraperitoneal administration. The irinotecan quantity in heart, kidneys, lungs, spleen, liver and tumor was explored through HPLC analysis and expressed as nanograms of drug per gram of organ (Figure 10).

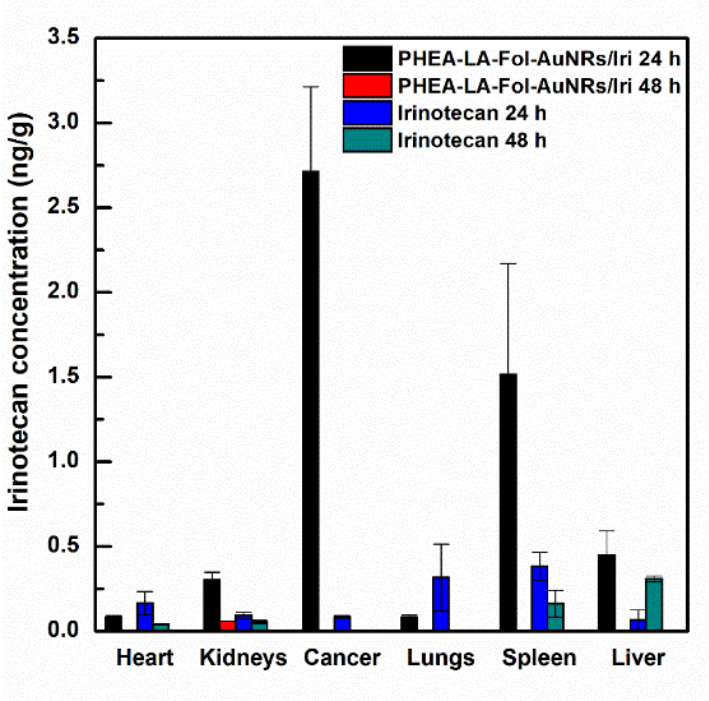

Figure 10. Irinotecan biodistribution 24h and 48h after intraperitoneal injection of PHEA-LA-Fol-AuNRs/Iri (24h – black; 48h – red) and irinotecan (24h – blue; 48h – green).

As expected, the highest amount of drug (2.7 ng/g) was found in tumor, 24h after PHEA-LA-Fol-AuNRs/Iri injection, underlining the capability of nanorods to preferentially accumulate in xenografts. Not surprisingly, noticeable values were also registered at the same timepoint in spleen and liver. These two findings strongly suggest that PHEA-LA-Fol-AuNRs/Iri might be able to deliver irinotecan via passive targeting. In particular, the most relevant biodistribution sites coincide with the ones presenting a discontinuous vasculature, which is known to allow the passive permeation of nanometric particles. On the other hand, low drug concentrations were found in cancers harvested 24h after the irinotecan injection, whereas the main accumulation sites resulted spleen and lungs. irinotecan was not detected at 48h post PHEA-LA-Fol-AuNRs/Iri injection, in any sample analyzed, except in kidneys. A possible explanation to this finding might be the occurrence of carboxylesterase-mediated drug hydrolysis. As reported elsewhere (Sanghani et al., 2003; Wang et al., 2018), carboxylesterases are not exclusively found in liver and they are as well expressed in other districts such as colon, heart, kidneys and human colon tumor tissue. It is reasonable to suppose that the high amount of irinotecan detected in tumor at day 1 was been rapidly hydrolyzed by carboxylesterase during the next 24h. A similar trend is appreciable in the rest of the organs analyzed.

3.6. Histology and Immunohistochemistry

Histological analysis of tumor sections of HCT116 xenografts treated with gold nanorods and the 810 nm cold laser beam revealed distinct alterations of tumor cell viability (Figure 11).

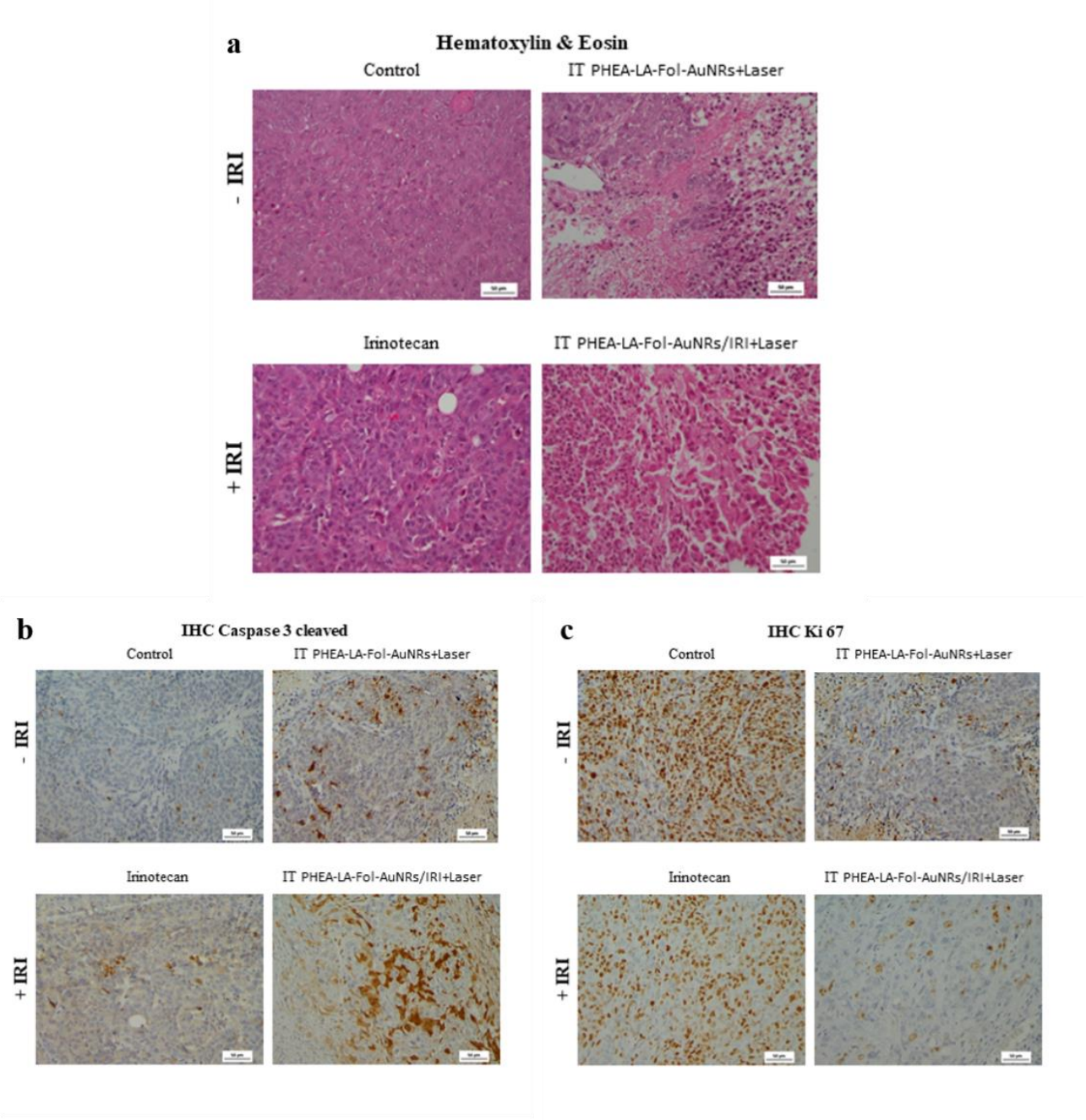

Figure 11. Histology and Immunohistochemistry stainings. a) Hematoxylin-eosin. b) IHC Caspase 3 cleaved apoptosis marker. c) IHC Ki 67 proliferation marker. Scale bar 50 µm.

Histological findings of PHEA-LA-Fol-AuNRs group receiving laser treatment showed extended regions of necrotic tissue (Figure 11a), even though vital areas were still present; while in groups treated with irinotecan, apoptotic cells were observed. Necrosis was characterized by loss of cellular detail, cell and nuclear swelling, pale cytoplasm, associated with cellular debris. Sometimes necrotic cells showed also nuclear dissolution (karyolysis) and nuclear fragments (karyorrhexis). Apoptotic

cells were smaller than the surrounding ones with a small pyknotic nucleus (due to chromatin condensation) and hypereosinophilic cytoplasm (due to cytoplasmic condensation). Microscopic findings for the tumor cells in the PHEA-LA-Fol-AuNRs/Iri + Laser group revealed both apoptosis and necrosis with cells that were large and swollen with pale eosinophilic cytoplasm and karyolysis (necrosis), whereas the apoptotic cells are small and shrunken with hypereosinophilic cytoplasm and pyknotic/fragmented nuclei. Untreated tumours consisted of viable, unaltered tissue without strong signs of apoptosis or necrosis (Figure 11a).

Immunohistochemical analyses were performed using sections of tumors removed from mice of all groups. Analyses conducted on sections of tumors of some groups are reported in Figure 11 b-c. Quantitative analyses (Figure 12) performed by ImageJ demonstrated that PHEA-LA-Fol-AuNRs (intratumor) with irinotecan and laser treatment markedly reduced the level of Ki67, which is involved in cellular proliferation, while level of Caspase-3 cleaved was markedly increased in the same group. Actually, the expression of cleaved caspase-3 is associated to the apoptotic pathway before DNA fragmentation, and is the best signaling event recognized in cell apoptosis (Belloc et al., 2000). High levels of active caspase-3-positive cells are strongly correlated with irinotecan-induced apoptosis; while in groups with laser treatment necrosis is the main histologic lesion.

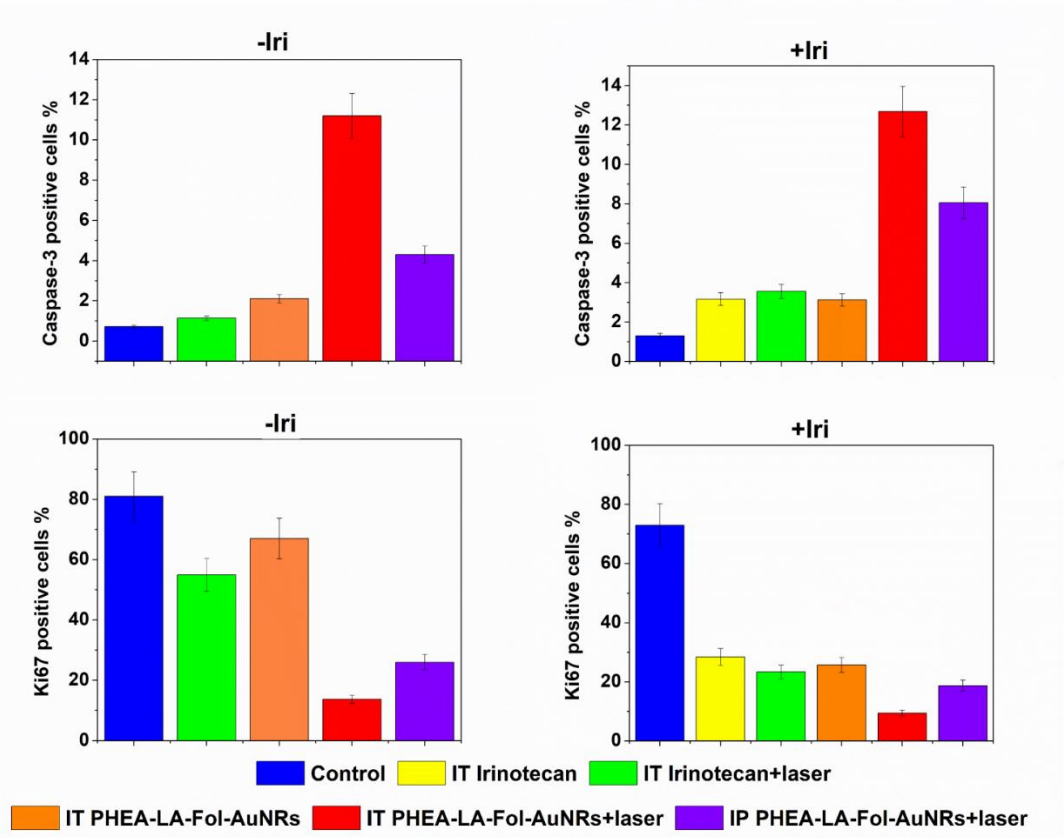

Figure 12. Immunohistochemistry quantitative analysis. Data indicate the number of positive cells in Caspase 3 and Ki 67 immunohistochemistry. Data are expressed as means ±SD.

4. Conclusions

In this study, the polymeric derivative PHEA-LA-PEG-FA was synthesized and used as stabilizing agent of gold nanorods to produce PHEA-LA-Fol-AuNRs. The antineoplastic drug irinotecan was then successfully embedded into the coated gold colloids, generating the nano drug delivery system PHEA-LA-Fol-AuNRs/Iri. Irinotecan-loaded nanorods showed a great stability overtime and an excellent ability to release the drug payload in slightly acidic environment, as well as in neutral medium. Laser-assisted hyperthermia studies revealed that empty and loaded constructs are capable to cause a noteworthy rising in temperature which increase along with gold concentration. PHEA-LA-Fol-AuNRs/Iri and irinotecan demonstrate a comparable cytotoxic effect on human colon cancer (HCT116) cell line. More interestingly, *in vivo* studies on Fox1nu/nu mice, highlighted the

exceptional capability of both empty and loaded nanoparticles to strongly decrease the tumor growth, after laser irradiation, achieving complete tumor eradication in case of PHEA-LA-Fol-AuNRs/Iri intratumoral administration. Nanometric size and folate decoration allow the nanoparticles preferential accumulation in the tumor, conceivably in virtue of the additive contribution of passive and active targeting mechanisms. Immunohistochemistry results showed a Caspase 3 expression increased in PHEA-LA-Fol-AuNRs/Iri group treated with laser, while Ki 67 was lower. Hence, laser-hyperthermia depleted the proliferative activity of treated tumors, which was macroscopically observed as tumor volume reduction. Taking into account the encouraging results obtained, PHEA-LA-Fol-AuNRs and PHEA-LA-Fol-AuNRs/Iri appear to be potential convincing tools in hyperthermia-driven colon cancer treatment.

Acknowledgements

Authors thank Italian MIUR (Ministero dell'Istruzione, dell'Università e della Ricerca) and University of Palermo for financial support;

ATeN Center of University of Palermo –Laboratory of preparation and analysis of biomaterials for scanning electron microscopy analysis.

Declarations of interest: none

References

Belloc, F., Belaud-Rotureau, M.A., Lavignolle, V., Bascans, E., Braz-Pereira, E., Durrieu, F., Lacombe, F., 2000. Flow cytometry detection of caspase 3 activation in preapoptotic leukemic cells. Cytometry 40, 151–160. https://doi.org/10.1002/(SICI)1097-0320(20000601)40:2<151::AID-CYTO9>3.0.CO;2-9

Camerin, M., Rello, S., Villanueva, A., Ping, X., Kenney, M.E., Rodgers, M.A.J., Jori, G., 2005. Photothermal sensitisation as a novel therapeutic approach for tumours: Studies at the cellular and animal level. Eur. J. Cancer 41, 1203–1212. https://doi.org/10.1016/j.ejca.2005.02.021

Castelli, F., Pitarresi, G., Giammona, G., 2000. Influence of different parameters on drug release from hydrogel systems to a biomembrane model. Evaluation by differential scanning calorimetry technique. Biomaterials 21, 821–33. https://doi.org/10.1016/s0142-9612(99)00252-5

Cavallaro, G., Triolo, D., Licciardi, M., Giammona, G., Chirico, G., Sironi, L., Dacarro, G., Donà, A., Milanese, C., Pallavicini, P., 2013. Amphiphilic Copolymers Based on Poly[(hydroxyethyl)-d , l -aspartamide]: A Suitable Functional Coating for Biocompatible Gold Nanostars. Biomacromolecules 14, 4260–4270. https://doi.org/10.1021/bm401130z

Chen, F., Cai, W., 2015. Nanomedicine for targeted photothermal cancer therapy: Where are we now? Nanomedicine. https://doi.org/10.2217/nnm.14.186

Chen, Y., Bian, X., Aliru, M., Deorukhkar, A.A., Ekpenyong, O., Liang, S., John, J., Ma, J., Gao, X., Schwartz, J., Singh, P., Ye, Y., Krishnan, S., Xie, H., 2018. Hypoxia-targeted gold nanorods for cancer photothermal therapy. Oncotarget 9, 26556–26571. https://doi.org/10.18632/oncotarget.25492

Craparo, E.F., Porsio, B., Mauro, N., Giammona, G., Cavallaro, G., 2015. Polyaspartamide-Polylactide Graft Copolymers with Tunable Properties for the Realization of Fluorescent

Nanoparticles for Imaging. Macromol. Rapid Commun. 36, 1409–1415. https://doi.org/10.1002/marc.201500154

Craparo, E.F., Sardo, C., Serio, R., Zizzo, M.G., Bondì, M.L., Giammona, G., Cavallaro, G., 2014. Galactosylated polymeric carriers for liver targeting of sorafenib. Int. J. Pharm. 466, 172–180. https://doi.org/10.1016/j.ijpharm.2014.02.047

Fiorica, C., Mauro, N., Pitarresi, G., Scialabba, C., Palumbo, F.S., Giammona, G., 2017. Double-Network-Structured Graphene Oxide-Containing Nanogels as Photothermal Agents for the Treatment of Colorectal Cancer. Biomacromolecules 18, 1010–1018. https://doi.org/10.1021/acs.biomac.6b01897

Fuchs, C., Mitchell, E.P., Hoff, P.M., 2006. Irinotecan in the treatment of colorectal cancer. Cancer Treat. Rev. 32, 491–503. https://doi.org/10.1016/j.ctrv.2006.07.001

Fujita, K., Kubota, Y., Ishida, H., Sasaki, Y., 2015. Irinotecan, a key chemotherapeutic drug for metastatic colorectal cancer. World J. Gastroenterol. 21, 12234–48. https://doi.org/10.3748/wjg.v21.i43.12234

Gao, J., Huang, X., Liu, H., Zan, F., Ren, J., 2012. Colloidal stability of gold nanoparticles modified with thiol compounds: Bioconjugation and application in cancer cell imaging. Langmuir 28, 4464–4471. https://doi.org/10.1021/la204289k

Gobin, A.M., Watkins, E.M., Quevedo, E., Colvin, V.L., West, J.L., 2010. Near-Infrared-Resonant Gold/Gold Sulfide Nanoparticles as a Photothermal Cancer Therapeutic Agent. Small 6, 745–752. https://doi.org/10.1002/smll.200901557

Grönbeck, H., Curioni, A., Andreoni, W., 2000. Thiols and disulfides on the Au(111) surface: The headgroup-gold interaction. J. Am. Chem. Soc. 122, 3839–3842. https://doi.org/10.1021/ja993622x

Hildebrandt, B., Wust, P., Ahlers, O., Dieing, A., Sreenivasa, G., Kerner, T., Felix, R., Riess, H., 2002. The cellular and molecular basis of hyperthermia. Crit. Rev. Oncol. Hematol. 43, 33–56.

Jiang, B.-P., Hu, L.-F., Wang, D.-J., Ji, S.-C., Shen, X.-C., Liang, H., 2014. Graphene loading water-soluble phthalocyanine for dual-modality photothermal/photodynamic therapy via a one-step method. J. Mater. Chem. B 2, 7141–7148. https://doi.org/10.1039/C4TB01038H

Jori, G., Spikes, J.D., 1990. Photothermal sensitizers: possible use in tumor therapy. J. Photochem. Photobiol. B. 6, 93–101.

Kumar, A., Mandal, S., Selvakannan, P.R., Pasricha, R., Mandale, A.B., Sastry, M., 2003. Investigation into the interaction between surface-bound alkylamines and gold nanoparticles. Langmuir 19, 6277–6282. https://doi.org/10.1021/la034209c

Lepock, J.R., 2003. Cellular effects of hyperthermia: relevance to the minimum dose for thermal damage. Int. J. Hyperth. 19, 252–266. https://doi.org/10.1080/0265673031000065042

Li, S.-D., Huang, L., 2010. Stealth nanoparticles: high density but sheddable PEG is a key for tumor targeting. J. Control. Release 145, 178–81. https://doi.org/10.1016/j.jconrel.2010.03.016

Li Volsi, A., Fiorica, C., D'Amico, M., Scialabba, C., Palumbo, F.S., Giammona, G., Licciardi, M., 2018. Hybrid Gold/Silica/Quantum-Dots supramolecular-nanostructures encapsulated in polymeric micelles as potential theranostic tool for targeted cancer therapy. Eur. Polym. J. 105, 38–47. https://doi.org/10.1016/J.EURPOLYMJ.2018.05.013

Li Volsi, A., Scialabba, C., Vetri, V., Cavallaro, G., Licciardi, M., Giammona, G., 2017. Near-Infrared Light Responsive Folate Targeted Gold Nanorods for Combined Photothermal-Chemotherapy of Osteosarcoma. ACS Appl. Mater. Interfaces 9, 14453–14469. https://doi.org/10.1021/acsami.7b03711

Liang, C., Diao, S., Wang, C., Gong, H., Liu, T., Hong, G., Shi, X., Dai, H., Liu, Z., 2014. Tumor

Metastasis Inhibition by Imaging-Guided Photothermal Therapy with Single-Walled Carbon Nanotubes. Adv. Mater. 26, 5646–5652. https://doi.org/10.1002/adma.201401825

Licciardi, M., Scialabba, C., Cavallaro, G., Sangregorio, C., Fantechi, E., Giammona, G., 2013a. Cell uptake enhancement of folate targeted polymer coated magnetic nanoparticles. J. Biomed. Nanotechnol. 9, 949–64.

Licciardi, M., Scialabba, C., Fiorica, C., Cavallaro, G., Cassata, G., Giammona, G., 2013b. Polymeric Nanocarriers for Magnetic Targeted Drug Delivery: Preparation, Characterization, and in Vitro and in Vivo Evaluation. Mol. Pharm. 10, 4397–4407. https://doi.org/10.1021/mp300718b

Lovell, J.F., Jin, C.S., Huynh, E., Jin, H., Kim, C., Rubinstein, J.L., Chan, W.C.W., Cao, W., Wang, L. V., Zheng, G., 2011. Porphysome nanovesicles generated by porphyrin bilayers for use as multimodal biophotonic contrast agents. Nat. Mater. 10, 324–332. https://doi.org/10.1038/nmat2986

Lowery, A.R., Gobin, A.M., Day, E.S., Halas, N.J., West, J.L., 2006. Immunonanoshells for targeted photothermal ablation of tumor cells. Int. J. Nanomedicine 1, 149–54.

Maeda, H., Matsumura, Y., 1989. Tumoritropic and lymphotropic principles of macromolecular drugs. Crit. Rev. Ther. Drug Carrier Syst.

Matsumura, Y., Maeda, H., 1986. A New Concept for Macromolecular Therapeutics in Cancer Chemotherapy: Mechanism of Tumoritropic Accumulation of Proteins and the Antitumor Agent Smancs. Cancer Res. 46, 6387–6392.

Mauro, N., Campora, S., Adamo, G., Scialabba, C., Ghersi, G., Giammona, G., 2016. Polyaminoacid-doxorubicin prodrug micelles as highly selective therapeutics for targeted cancer therapy. RSC Adv. 6, 77256–77266. https://doi.org/10.1039/C6RA14935A

Mauro, N., Li Volsi, A., Scialabba, C., Licciardi, M., Cavallaro, G., Giammona, G., 2017.

Photothermal Ablation of Cancer Cells Using Folate-Coated Gold/ Graphene Oxide Composite. Curr. Drug Deliv. 14, 433–443. https://doi.org/10.2174/1567201813666160520113804

Mauro, Nicolò, Li Volsi, A., Scialabba, C., Licciardi, M., Cavallaro, G., Giammona, G., 2016. Photothermal Ablation of Cancer Cells Using Folate-Coated Gold/ Graphene Oxide Composite. Curr. Drug Deliv. 13.

Melancon, M.P., Zhou, M., Li, C., 2011. Cancer Theranostics with Near-Infrared Light-Activatable Multimodal Nanoparticles. Acc. Chem. Res. 44, 947–956. https://doi.org/10.1021/ar200022e

Mendichi, R., Giacometti Schieroni, A., Cavallaro, G., Licciardi, M., Giammona, G., 2003. Molecular characterization of α,β-poly(N-2-hydroxyethyl)-dl-aspartamide derivatives as potential self-assembling copolymers forming polymeric micelles. Polymer (Guildf). 44, 4871–4879. https://doi.org/10.1016/S0032-3861(03)00486-5

O'Neal, D.P., Hirsch, L.R., Halas, N.J., Payne, J.D., West, J.L., 2004. Photo-thermal tumor ablation in mice using near infrared-absorbing nanoparticles. Cancer Lett. 209, 171–176. https://doi.org/10.1016/J.CANLET.2004.02.004

Parker, N., Turk, M.J., Westrick, E., Lewis, J.D., Low, P.S., Leamon, C.P., 2005. Folate receptor expression in carcinomas and normal tissues determined by a quantitative radioligand binding assay. Anal. Biochem. 338, 284–293. https://doi.org/10.1016/J.AB.2004.12.026

Pensa, E., Cortés, E., Corthey, G., Carro, P., Vericat, C., Fonticelli, M.H., Benítez, G., Rubert, A.A., Salvarezza, R.C., 2012. The chemistry of the sulfur-gold interface: In search of a unified model. Acc. Chem. Res. 45, 1183–1192. https://doi.org/10.1021/ar200260p

Qiu, W.X., Liu, L.H., Li, S.Y., Lei, Q., Luo, G.F., Zhang, X.Z., 2017. ACPI Conjugated Gold Nanorods as Nanoplatform for Dual Image Guided Activatable Photodynamic and Photothermal Combined Therapy In Vivo. Small 13, 1603956. https://doi.org/10.1002/smll.201603956

Reddy, J.A., Low, P.S., 1998. Folate-mediated targeting of therapeutic and imaging agents to cancers. Crit. Rev. Ther. Drug Carrier Syst. 15, 587–627.

Sanghani, S.P., Quinney, S.K., Fredenburg, T.B., Sun, Z., Davis, W.I., Murry, D.J., Cummings, O.W., Seitz, D.E., Bosron, W.F., 2003. Carboxylesterases expressed in human colon tumor tissue and their role in CPT-11 hydrolysis. Clin. Cancer Res. 9, 4983–91.

Sinha, R., Kim, G.J., Nie, S., Shin, D.M., 2006. Nanotechnology in cancer therapeutics: bioconjugated nanoparticles for drug delivery. Mol. Cancer Ther. 5, 1909–1917. https://doi.org/10.1158/1535-7163.MCT-06-0141

Sortino, S., 2012. Photoactivated nanomaterials for biomedical release applications. J. Mater. Chem. 22, 301–318. https://doi.org/10.1039/C1JM13288A

Turkevich, J., Stevenson, P.C., Hillier, J., 1951. A study of the nucleation and growth processes in the synthesis of colloidal gold. Discuss. Faraday Soc. 11, 55. https://doi.org/10.1039/df9511100055

Wang, D., Zou, L., Jin, Q., Hou, J., Ge, G., Yang, L., 2018. Human carboxylesterases: a comprehensive review. Acta Pharm. Sin. B 8, 699–712. https://doi.org/10.1016/j.apsb.2018.05.005

Wang, S., Riedinger, A., Li, H., Fu, C., Liu, H., Li, L., Liu, T., Tan, L., Barthel, M.J., Pugliese, G., De Donato, F., Scotto D'Abbusco, M., Meng, X., Manna, L., Meng, H., Pellegrino, T., 2015. Plasmonic Copper Sulfide Nanocrystals Exhibiting Near-Infrared Photothermal and Photodynamic Therapeutic Effects. ACS Nano 9, 1788–1800. https://doi.org/10.1021/nn506687t

Weissleder, R., 2001. A clearer vision for in vivo imaging. Nat. Biotechnol. 19, 316–317. https://doi.org/10.1038/86684

Yang, L., Tseng, Y.T., Suo, G., Chen, L., Yu, J., Chiu, W.J., Huang, C.C., Lin, C.H., 2015. Photothermal therapeutic response of cancer cells to aptamer-gold nanoparticle-hybridized graphene oxide under NIR illumination. ACS Appl. Mater. Interfaces 7, 5097–5106. https://doi.org/10.1021/am508117e

Yu, M., Guo, F., Wang, J., Tan, F., Li, N., 2016. A pH-Driven and photoresponsive nanocarrier: Remotely-controlled by near-infrared light for stepwise antitumor treatment. Biomaterials 79, 25–35. https://doi.org/10.1016/j.biomaterials.2015.11.049

Zhang, A., Guo, W., Qi, Y., Wang, J., Ma, X., Yu, D., 2016. Synergistic Effects of Gold Nanocages in Hyperthermia and Radiotherapy Treatment. Nanoscale Res. Lett. 11, 279. https://doi.org/10.1186/s11671-016-1501-y

Zhang, Jimei, Li, C., Zhang, Xu, Huo, S., Jin, S., An, F.-F., Wang, X., Xue, X., Okeke, C.I., Duan, G., Guo, F., Zhang, Xiaohong, Hao, J., Wang, P.C., Zhang, Jinchao, Liang, X.-J., 2015. In vivo tumor-targeted dual-modal fluorescence/CT imaging using a nanoprobe co-loaded with an aggregation-induced emission dye and gold nanoparticles. Biomaterials 42, 103–111. https://doi.org/10.1016/j.biomaterials.2014.11.053

Zou, L., Wang, H., He, B., Zeng, L., Tan, T., Cao, H., He, X., Zhang, Z., Guo, S., Li, Y., 2016. Current Approaches of Photothermal Therapy in Treating Cancer Metastasis with Nanotherapeutics. Theranostics 6, 762–72. https://doi.org/10.7150/thno.14988